A Comparative Study of Miniature Capsule Designs and their ability to Translate Magnetic Energy into Work

E.A.Codrea

University of Twente, Faculty of Engineering Technology, Drienerlolaan 5, 7522 NB, Enschede, The Netherlands
E.A.Codrea@student.utwente.nl

ABSTRACT: Tetherless robots are an important step in developing a new generation of miniature capsule as they allow for non-invasive procedures, which also permit more detailed exploration of the gastro-intestinal track. In this research paper designs for such capsules are realized with the aim of replacing current endoscopic capsules for non-invasive procedures. These designs are then optimized according to design parameters. A comparison is then made, between designs, observing which is better able to translate magnetic energy into work. Using Resistive Force Theory and Oldroyd-B mathematical models, velocities are derived for a helical and screw milli-robot design, as well as magnetic field being constructed with a field strength between 100-300 mT. Optimal designs based on the models are generated for screw and helix milli-robots, taking into consideration physical design parameters, with the goal of maximizing velocity. The paper is then able to conclude using numerical analysis a helix design is able to produce more work.

Key words: Endoscopic Capsule, Magnetic Field, Milli-Robot, Resistive Force Theory, Oldroyd-B

1 INTRODUCTION

Medical professionals have long envisioned making surgeries as painless as possible, and with minimum negative long term effects. Minimally invasive procedures and milli-robots being developed aid in steps towards that direction. Non-invasive procedures have the benefit of reducing recovery time, post operative care, as well as minimizing the amount of medical complications encountered within procedures [1].
Medical capsules are used in endoscopies, for exploring the gastro-intestinal (GI) track. Current medical standards are of two types. The first method works by using invasive endoscopic procedures where a camera along a tube is placed through the trachea of the patient. The camera then has the ability to be moved around to carefully observe the walls of the intestine. However, this method can be damaging to the body and is uncomfortable to the patient. As well, such an approach is not able to reach all regions of the intestine due to the endoscope being tethered. The second method works by using robots with cameras that resemble pills. These robots are swallowed and using peristalsis (muscle contractions that move items through the GI track) are able to take videos/pictures as they travel through the body. When medical experts review such footage, often times they do not have a complete image as the robot moves uni-directionally along the track. The non-invasive method has no options to be able to move the robot to review the surroundings more carefully [2].
Currently novel milli-robot are being developed that would combine the non-invasiveness of the pill form with the ability to move, and view desired areas. Overall, being able to explore the GI tract more extensively. This new type of milli-robot aims to be able to be use standard MRI technology to navigate an induced non-uniform directional magnetic field to explore the body [3].
This paper aims to create designs based on helix and screw milli-robots, a test-setup that can be used to simulate a low-Reynolds number environment with a magnetic field, and then observe which design is best able to convert magnetic energy into work. Robots will be modeled through Resistive Force Theory and Oldroyd-B mathematical models respectively. Optimal values, given the design parameters, are to be search for in each milli-robot design. Once said values are found, the research question to be answered is which milli-robots designs are better able to translate magnetic energy into work.

1.1 Background Information on Milli-Robots

Robots for endoscopic procedures are modeled after bacterial flagella, this is due to the low Reynolds-number environment in which they must function. Given that nature has developed a locomotion method

for such environments, current state of the art aims to mimic bacteria to be able to achieve controlled motion in such situations. Currently there is a struggle to miniaturize such motor systems, as a result magnetic fields are used to initialize movement. State of the art contains two types of robots, soft and rigid body. Rigid body robots are easier to manufacture, and as such are the focus of the paper. Rigid body, flagella robots, can be broken into roughly three categories themselves: screw, helix, and twist propellers. The research paper will focus on screw and helix propeller designs as they are the two most varied in between each other [4].

2 METHODS: MATHEMATICAL MODELS

To better understand the design choices made later on, it is important to first see which variables affect helix and screw shaped propellers. The helix propeller is based on a Resistive Force Theory model, while the screw is based on an Oldroyd-B model. The linear and angular velocity for both models is derived according to variables related to design choices. Those values are used to create an optimal designs for the robots.

2.1 Magnetic Torque

The tri-axial coils designed for the milli-robots use magnetic actuation so that they may be able to generate a magnetic torque. This torque will be used to rotate the body in which the coils are encompassed.

$$\boldsymbol{\tau_m} = \mathbf{m} \times \mathbf{B} = -Sk(\mathbf{B})\mathbf{m}. \tag{1}$$

$$Sk(\begin{bmatrix} n_1 \\ n_2 \\ n_3 \end{bmatrix}) = \begin{bmatrix} 0 & -n_3 & n_2 \\ n_3 & 0 & -n_1 \\ -n_2 & n_1 & 0 \end{bmatrix}. \tag{2}$$

The magnetic torque is obtained through the cross product of the magnetic moment (**m**) and field (**b**). We replace **B** with its skew symmetric matrix to make calculations easier, and be able to obtain the torque in matrix form. This technique is shown in equation (2).

$$\mathbf{m} = N\mathbf{I}S. \tag{3}$$

Looking further into the magnetic moment it can be broken down as the product of: the number of turns of the coil N, the current flowing through the coil **I**, and the vector area S.

2.2 Stokes Drag of a sphere and cylinder

Stokes drag is used because the objects observed will be simulated for a low Reynolds environment. The formula for the stokes drag of a sphere is used for the helical design as the components will be stored in such a body. The same formula is also used for the cylinder. This is because for Stoke's drag the coefficient at low Reynolds-numbers for a cylinder is the same as for a sphere [5].

$$\boldsymbol{\omega} = \frac{1}{\pi d^3 \mu}\boldsymbol{\tau}_m. \tag{4}$$

To obtain the angular velocity shown in equation (4), a Stoke's drag formula derived from [6] is used for both proposed designs.

2.3 Helix Shaped Propeller

The derivation for the velocity begins using the unit tangent vector **t**, the unit normal vector **n** and the binormal vector **b** as defined [7].

$$\begin{aligned} \mathbf{t} &= \frac{dx(s,t)/ds}{|dx(s,t)/ds|}. \\ \mathbf{n} &= \frac{dt/ds}{|dt/ds|} = \frac{1}{k}\frac{dt}{ds}. \\ \mathbf{b} &= \mathbf{t} \times \mathbf{n}. \\ k &= |\frac{dt}{ds}|. \end{aligned} \tag{5}$$

The vectors in equation (5) are what comprise the Frenet basis along the length of helix according to a time t. However, since the body is assumed to be rigid the result is that these equations are independent of time. Equation (5) also shows the 3-D curvature k, which showcases how the curve bends in a 3 dimensional space.

$$\mathbf{x}(s) = [R\cos(s), R\sin(s), hs]. \tag{6}$$

Equation (6) describes the shape of the helix in the x,y,z axis. The helix shape is parametrized from $0 \leq s < 2\pi$, one full rotation.

$$\begin{aligned} \mathbf{t} &= \frac{[-R\sin(s), R\cos(s), h]}{\sqrt{R^2+h^2}}. \\ \mathbf{n} &= [-\cos(s), -\sin(s), 0]. \\ \mathbf{b} &= \frac{h}{\sqrt{R^2+h^2}}[\sin(s), -\cos(s), \frac{R}{h}]. \end{aligned} \tag{7}$$

Deriving equation (6) according to the formulae in equation (5) then presents the Frenet basis seen in equation (7), where $k = R/\sqrt{R^2 + h^2}$.

$$\mathbf{R} = [\mathbf{t}, \mathbf{n}, \mathbf{b}]. \tag{8}$$

The full Frenet frame is assembled as equation (8). This is done based on the following work [8].

$$\begin{aligned} \delta\mathbf{f}_{||} &= -\boldsymbol{\xi}_{||}\mathbf{U}_{||}\delta l. \\ \delta\mathbf{f}_{\perp} &= -\boldsymbol{\xi}_{\perp}\mathbf{U}_{\perp}\delta l. \\ \delta\mathbf{f}_{\vdash} &= -\boldsymbol{\xi}_{\vdash}\mathbf{U}_{\vdash}\delta l. \end{aligned} \tag{9}$$

Writing the equations of motion for the force of a helix about its length is presented as equation (9), where the forces are split into a tangent, normal, and binormal component. Each formula contains a drag matrix showcasing how it moves inside the fluid at a specific velocity along any point on the helix.

$$\left[\boldsymbol{\xi}\right] = \begin{bmatrix} L\frac{2\pi\mu}{ln(0.18/R_t)} & 0 & 0 \\ 0 & L\frac{4\pi\mu}{ln(0.18/R_t+0.5)} & 0 \\ 0 & 0 & L\frac{4\pi\mu}{ln(0.18/R_t)} \end{bmatrix}. \tag{10}$$

The fully assembled drag matrix for a helix moving at low Reynolds-numbers is seen in equation (10), where μ represents the viscosity of the fluid [9].

$$\delta\mathbf{f} = -\mathbf{R}\boldsymbol{\xi}\mathbf{R}^T\mathbf{U}\delta l. \tag{11}$$

Using the Frenet frame, the forces and velocities presented in (9) for the shape of a helix can be mapped out. Further on, this will yield the force drag equation according to its frame as presented above in equation (11) [8].

$$\mathbf{r} = \begin{bmatrix} R\cos(s) - \frac{6h^2R}{3R^2+4\pi^2h^2} \\ R\sin(s) + \frac{6h^2R}{3R^2+4\pi^2h^2} \\ hs - \frac{3\pi h^2R^2+6\pi h^2}{3R^2+4\pi^2h^2} \end{bmatrix}. \tag{12}$$

The relative velocity vector $\mathbf{U}$ can be expanded into its transnational and rotational components as $\mathbf{U} = \mathbf{v} + \boldsymbol{\omega} \times \mathbf{r}$, where $\mathbf{r}$ represents the distance between the center of mass and an arbitrary point. For ease of calculation the vector $\mathbf{r}$ has been turned into a skew matrix, as was presented in equation (2). The $\mathbf{r}$ vector is shown in equation (12).

$$\begin{aligned} \begin{bmatrix} \mathbf{f} \\ \mathbf{M} \end{bmatrix} &= \begin{bmatrix} -\mathbf{R}\boldsymbol{\xi}\mathbf{R}^T & \mathbf{R}\boldsymbol{\xi}\mathbf{R}^T Sk(\mathbf{r}) \\ -Sk(\mathbf{r})\mathbf{R}\boldsymbol{\xi}\mathbf{R}^T & Sk(\mathbf{r})\mathbf{R}\boldsymbol{\xi}\mathbf{R}^T Sk(\mathbf{r}) \end{bmatrix} \begin{bmatrix} \mathbf{v}\delta l \\ \mathbf{w}\delta l \end{bmatrix} \\ &= \int_0^L \begin{bmatrix} \mathbf{R}_{11} & \mathbf{R}_{12} \\ \mathbf{R}_{21} & \mathbf{R}_{22} \end{bmatrix} \begin{bmatrix} \mathbf{v} \\ \mathbf{w} \end{bmatrix} \delta L. \end{aligned} \tag{13}$$

Once equation (11) is expanded and the same procedure is carried out for the moment equation, the full equation of motion presents itself as seen in equation (13). The total propulsive force and torque along the helix is obtained by integrating equation (13) over the total length of the helix.

$$\mathbf{v} = \mathbf{R}_{21}^{-1}[\mathbf{M} - \mathbf{R}_{22}\omega]. \tag{14}$$

By knowing the total amount of torque provided by the magnetic field to a coil, together with the angular velocity, the linear velocity of the helix is obtained in equation (14).

2.4 Screw Shaped Propeller

$$U = 2A\omega\epsilon^2 \sum_{q\geq 1} \frac{(1 + \beta q^2 De^2)|f_q|}{1 + q^2 De^2} J_q. \tag{15}$$

The main governing equation for the velocity of a Screw propeller is shown in equation (15), obtained from an Oldroyd-B model [10] [11] [12]. The equation dictates the design parameters for the velocity of a screw milli-robot. ω represents the angular velocity.

$$\begin{aligned} \epsilon &= \frac{t_d}{A}. \\ De &= \lambda\omega. \\ \beta &= \frac{\eta_s}{\eta}. \end{aligned} \tag{16}$$

ϵ represents the ratio of the arm depth (t_d) of the screw to that of the inner body. De is a variable known as Deborah's number and is defined as λ, representing the fluid relaxation timescale, multiplied by the angular velocity. Within the equation it is used to help define the fluidity of the material. β is defined as the ratio of solvent viscosity to the total viscosity. The

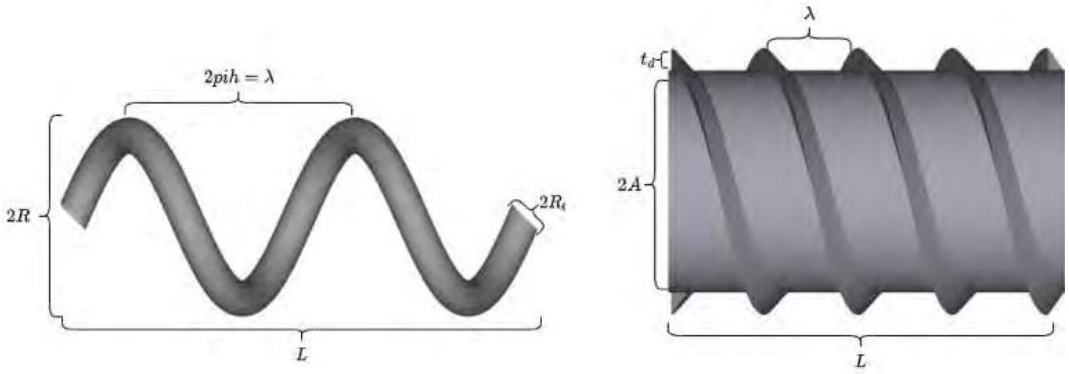

Fig. 1: Left Hand Side: Representation of helix body and its variables: R represents the inner radius around which the helix turns, $2\pi h$ is the height of a turn. L representing the length of the body, R_t representing the radius of the thickness of the wire. Right Hand Side: Representation of screw body and its variables: A is inner radius of the screw, λ is the wavelength, t_d is the arm depth, L is the total length of the body, N is the number of starts

variable q represents the absolute value of the Fourier transform expansion coefficients [10] [12].
The variable f_q is the Fourier series expansion coefficients for the periodic wave profile function $f(N\theta)$, where N dictates the number of wings which the screw has. J_q is calculated based on Bessel functions which are further elaborated in [11]. However, details of these equations are outside the scope of the paper.

2.5 Magnetic Modeling and Energy

The Python library MagPyLib was used to simulate magnets with the aim of finding the magnet which provided the necessary characteristics for the least amount of force, so as to not be a safety hazard.

$$E_{magnetic} = 2\mathbf{I}A\mathbf{B}. \tag{17}$$

To be able to find the magnetic energy provided by a system, equation (17) is required. The aforementioned equation takes into account the current of the coils **I**, the area of the magnet A, and the magnetic field experienced by the subject **B**.

2.6 Kinetic Energy and Work Calculations

$$E_K = \frac{1}{2}mv^2 + \frac{1}{2}\omega^2. \tag{18}$$

$$W = E_{magnetic} - E_{kinetic}. \tag{19}$$

Equations (18) and (19) show the calculation of kinetic energy in a low Reynolds-number environment and work respectively. To note is that for the formula of kinetic energy there is no inertia term. This is because in low Reynolds environments, inertia is no longer taken into account as it becomes too small.

3 RESULTS

3.1 Design of an Uniform Magnetic Field and Experimental Set-up

As previously mentioned in the introduction, the milli-robots discussed need a magnetic field from which they will be able to generate a magnetic torque to turn. To achieve such an effect, two strong magnets have been aligned parallel to each another. The key design parameters for the creation of the field were: the distance between the magnets, the shape of the magnets, as well as the strength of the magnets.
The requirement for the milli-robots to generate enough torque was for them to experience a magnetic field strength between 100 to 300 mT. Magnetic field strength decreases exponentially as distance increases. As such, the minimum magnetic field that the robot experiences is at the mid-point between the two magnets. The shape of the magnet was chosen to be cylindrical, as not only does the shape mean that it has a stronger magnetic field due to the poles having a larger surface area, but also because its shape more easily facilitates a symmetric magnetic field.
Based on these criteria, magnets were selected from Supermagnete.nl to avoid the need for speciality man-

ufacturing. Given the available magnets two S-70-35-N magnets were selected which could be up to 15 cm apart to provide a sufficient magnetic field strength.

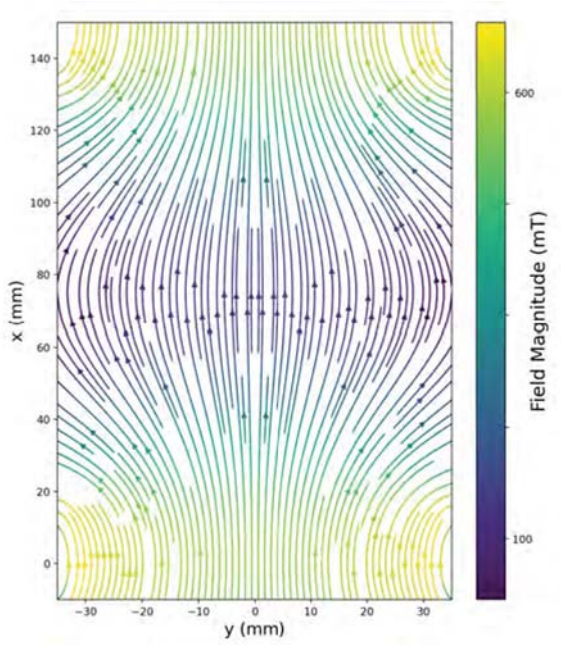

Fig. 2: Magnetic Field for two magnets, 10 cm apart , providing a minimum magnetic field strength of 100 mT at the mid-point

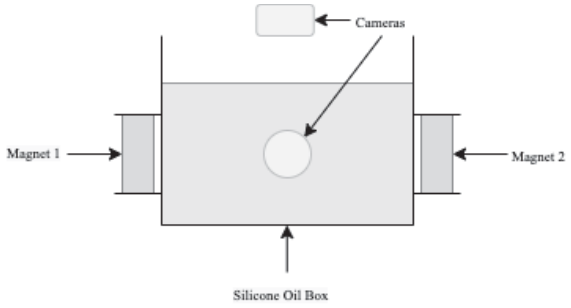

Fig. 3: Visual representation of the experimental setup

Figure 2 showcases a magnetic field where the two magnets are at a distance of 15 cm from one another. As expected the minimum magnetic field encountered is at the center of the test set-up with magnetic field strength rapidly increasing as it approaches the magnets themselves.

To answer the research question of which of the two milli-robot designs is better able to turn magnetic energy into work a method for data collection in necessary. Figure 3 showcases an experimental set-up designed to be able to experimentally analyze the milli-robot designs. The set-up contains two cameras, one with a front view and one with a top view. This cameras set-up can see how the milli-robot translates and rotates in all of its 6 degrees of freedom. Once data is collected, it will be analyzed using the footage to see how much the robot was able to move.

3.2 Design of Milli-Robots

Each milli-robot designed has two distinct parts to it: the component casing and the propeller. The current endoscopic capsule robot which the milli-robot aims to replace has a length of 25 mm and a thickness of 11 mm [13]. Making the new milli-robots the same size as the current capsule makes for them to be more easily implemented in the same use cases, due to similar measurements being present. Table 1 features the main electronics to be implemented into the milli-robots. Each design needs to ensure that it is able to contain all the necessary components for the robot to function. The mentioned components are used to create certain design constraints for each robot.

Table 1: Table of components within the milli-robots and their respective sizes in mm

Component	Length	Width	Height
Coils	6	6	9.2
Battery	11.5	11.5	3.1
Microchip	7	7	1
Magnetic Sensor	2.6	2.1	0.1
LED Driver	3	2.5	1
RF Transmitter	7	7	0.1

3.3 Design of Screw Component Placement

Delving into the screw milli-robot, the method by which the electronics will be integrated within the system is different. A helical propeller is a thin body which does not have the space to have components contained inside, however a screw has a closed central body which the thread surrounds. This will be used as an advantage since it allows for the electronics to be contained within the main body without the need for an additional capsule as the helical propeller does. The battery chosen for the robots is the largest component. As a screw milli-robot is circular, the container should at least be able to fit the battery with some spare space for placing components inside. Doing so assures that there is no need for an induced fit. An inner diameter of 12 mm is the design choice for

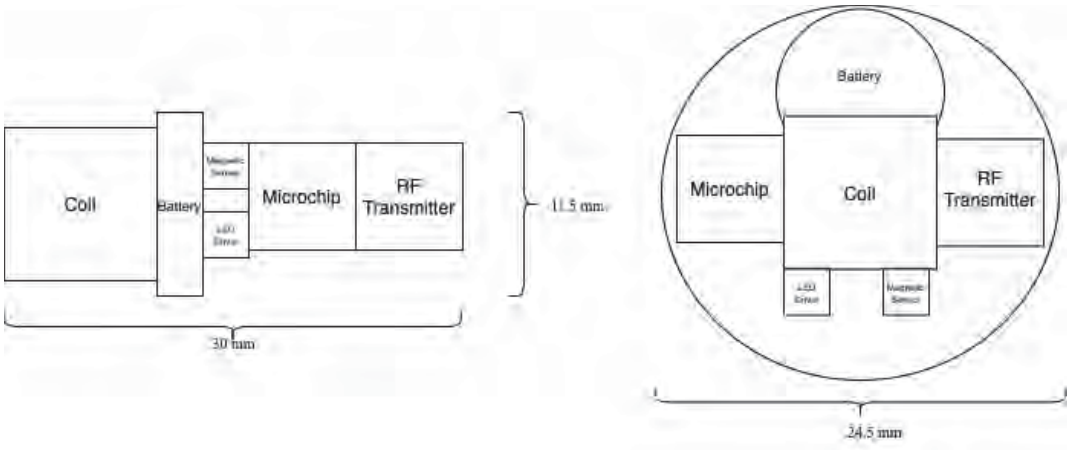

Fig. 4: Left Hand Side: Top View of the arrangement of all micro-electronic components lengthwise for a screw milli-robot. Right Hand Side: Top View of the arrangement of all components lengthwise for screw milli-robot

the minimum inner diameter of the screw robot so that space would exist for wiring and other miscellaneous placement. The length of the screw's central body has a range of possibilities depending on the arrangement of the micro-electronics. If all components are stacked as closely as possible, the minimum lengthwise arrangement would result in approximately 30 mm. Figure 4 showcases the most condensed component placement for a screw design.

Knowing these minimum size parameters, the maximum sizing also needs to be established. As mentioned the new milli-robot must be easily able to replace the existing endoscopic capsule. Mimicking the size constraints of the existing capsule is important so that the size a patient is expected to swallow stays the same. Due to this the capsule will be aimed to have no more than 10 mm added in total diameter and length from the minimum inner diameter and length requirement. The reason for this decision is that the capsule being built is scaled up from the finalized version. The final version is intended to be used with the magnetic field of an MRI, which has an average magnetic field strength of 1.5 T, which is over 100 times stronger than the current experimental setup. The above means that the final product could be scaled down further while producing similar results as experimental ones. Another fixed design factor is that the angle of the thread will be at 45° as that has been found to be the optimal angle to produce thrust [14].

3.4 Design of Helical Component Placement

As the helix milli-robot is not able to store its components within the body it requires a separate container for them. The container is shaped as a sphere due to the aerodynamicty of the shape, as well as its ability to encompass a large amount of objects in a compact shape. The sphere has a diameter of 24.5 mm and the components themselves will be housed as showcased in Figure 4.

3.5 Design of Screw Propeller

The screw propeller designs choices will be looked at more closely and optimized in terms of area, distance in between threads, arm depth, and number of arm. Angular velocity is fixed due to it being a result of the shape of the body and the magnetic torque. Viscosity is also fixed at 50 Pa s, as it is a result the medium chosen for the test set-up, silicone oil.

The first variable that is taken under consideration is the number of arms, which is chosen as an integer between 1 to 3. The reason why this design choice was made was because by having such a high number of arms it would limit arm depth and pitch options. If the number of arms would be increased past three, the screw would begin resembling a solid rigid body that no longer could produce thrust to drive itself forward. Over the course of testing variables the 3 wing types will be visualized. This is to show not only the relationship between a given variable and velocity, but to also be able to observe how increasing the number of arms affects the design.

A set of wavelength variables was chosen spanning

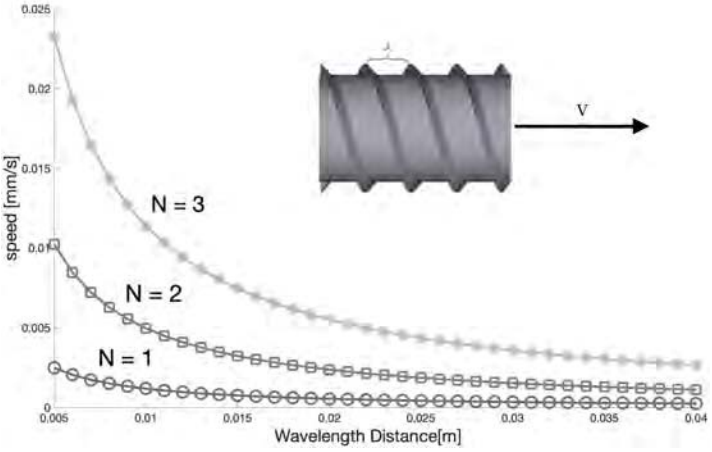

Fig. 5: Speed vs wavelength distance screw design graph, where speed drops as wavelength increases. Equation 15 is used to graph the figure.

from 1 mm to 40 mm, as that is the longest the screw is allowed to be. In Figure 5 it can be observed that as wavelength distance increases, the speed is observed to decrease. This relationship is almost exponentially for a higher wing number. The conclusion that can be drawn is that the higher the distance in between rotations of the screw, the slower the screw is able to translate forward. To note is that the higher the number of arms, the higher the speed; especially at the lowest distances.

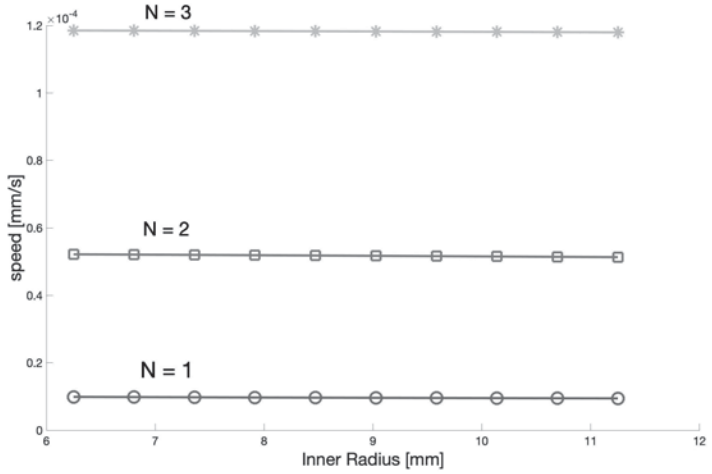

Fig. 6: Speed vs inner radius screw design graph, where speed has a slightly downwards trend as wavelength inner radius increases. Equation 15 is used to graph the figure.

The same process was done to look at the inner radius of the screw, with a fixed variable of 1 mm arm depth, as well as a fixed wavelength. In Figure 6 radius spans from 6.25 mm to 11.25 mm, as those were the minimum and maximum radius parameters respectively. The change as size increased was slightly linearly downwards, with not much change in slope. The conclusion that can be drawn is that a lower radius is beneficial, however it is not a dominant parameter for the dynamics of the screw. Yet again, more wings were more beneficial for the speed that the screw was able to obtain.

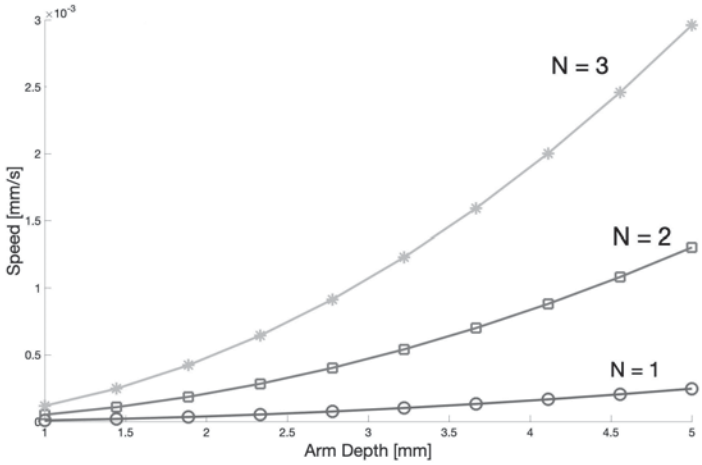

Fig. 7: Speed vs arm depth screw design graph, where speed rises almost exponentially as the arm depth increases. Equation 15 is used to graph the figure.

Changing the arm depth with a fixed wavelength, and arm depth gave an inverse relationship to that of the wavelength. As can be seen in Figure 7, the arm depth increased, there was an almost exponential upwards trend in speed; especially for a higher number of arms. The conclusions that can be drawn from the above family of graphs is, that to obtain an as optimal screw as possible, there needs to be a high arm depth, while maintaining a low wavelength and radius.
The aforementioned translates to having as high as possible normalized pitch, and by extension length, while maintaining a minimum diameter possible. Since the minimum diameter possible is that of 12.5 mm that is the one that will be kept. Given the remaining possible size, the arm depth will be increased to reach the maximum size possible, meaning that the arm depth will be of 5 mm. The number of arms was maximized to 3, and the pitch was minimized to 1 mm. The Final CAD design of the screw based on the above parameters can be observed in Figure 8.

3.6 Design of Helical Propeller

The starting equations for the design of the helical milli-robot are equation (14). There are four main de-

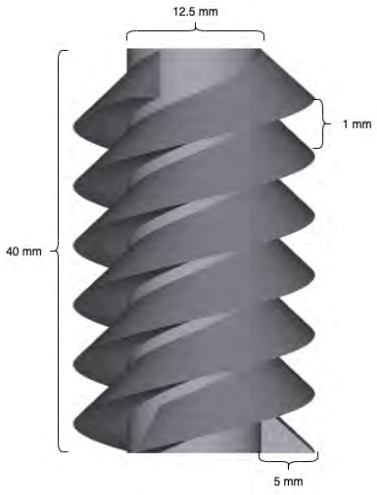

Fig. 8: Design of optimized screw milli-robot with length of 40 mm, arm depth of 5 mm, inner diameter of 12.5mm, and pitch of 1 mm.

sign variables in these equations: the radius around which the helix turns, height, number of turns, and the radius of the wire. Variables such as viscosity are known and fixed at 50 Pa s, the viscosity of silicone oil. The reason for this specific fluid is due to its high viscosity, and therefore aiding in making the simulation environment as close to that of the real one; a low Reynolds-number environment. As well the angle of the wire is fixed to 45° since that is the orientation in which it is best able to generate thrust [14].

To design the helix milli-robot propeller a range of variables is to be fixed. Since the helical propeller does not require any components be stored in it, the minimum requirements for the shape that will be tested are as low as can be possibly manufactured. The means that the turn radius, the height of a turn, and radius will all be of 1 mm. The length of the helical propeller is to be of minimum of 1 mm as well since that would make the full system the same size as the original capsule. The maximum values will be placed in such a way so that they match the ones of the screw milli-robot for a fair product evaluation. It is not only important to see which capsule is better at converting magnetic energy into work, but also at what size it is able to do so. As a result the length of the milli-robot is to be no longer than 40 mm, the total radius should not exceed 12.25 mm (including the thickness of the wire). Note that the thickness of the wire can not be greater or equal to πh as that would mean the helix would be a solid shell.

Looking at Figure 9 which analyzes the speed for

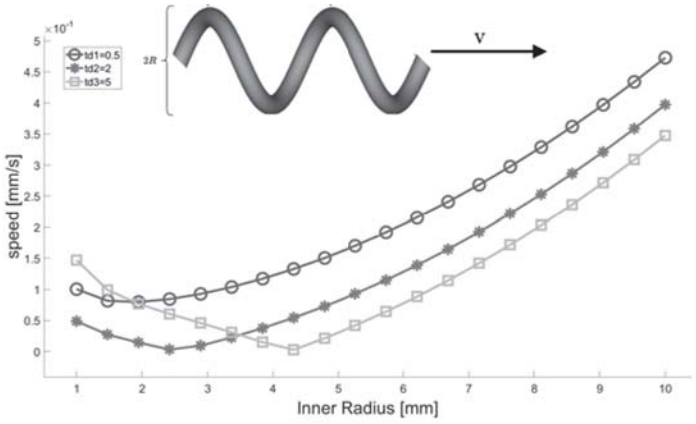

Fig. 9: Speed vs inner radius of helix design graph, for three different wire radii and fixed wavelength. Speed increases as radius increases. Equation 14 is used.

three values of wire thickness across a range of inner radii, and with a fixed h of 1 mm we can clearly see that having a larger inner radius is more beneficial to a helix propeller. As well from the above graph it can be seen that having a lower thickness is more beneficial to being able to generate speed. Another relationship that can be observed from the figure is that speed begins to grow after the inner radius becomes larger than the thickness of the wire itself. The figure only showcases the result for an h of 1 mm. However, a range of h values was tested and it was observed that speed grows faster when h is smaller.

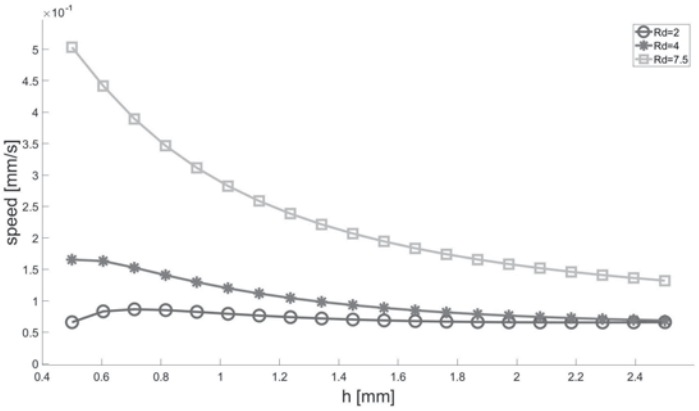

Fig. 10: Speed vs h, of helix design graph for three different inner radii and fixed wire radius. Speed decreases as h increases. Equation 14 is used.

The second analysis for the helical propeller can be seen in Figure 10, where the relationship of speed against h is plotted. Using a fixed thickness radius of 0.5 mm and three values of inner radius thickness, it can be seen that the aforementioned figure concurs

with Figure 9. Yet again it is more beneficial to have a higher inner radius, and more valuable to have a lower h value. This makes sense physically as well as having a lower h allows for the helix wire to more often interact with the environment and therefore more easily generate thrust.

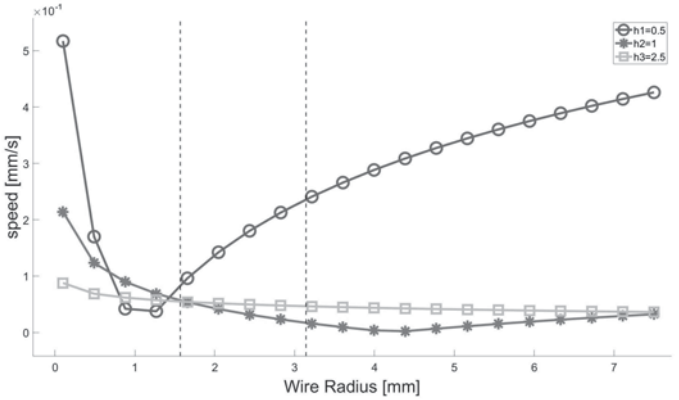

Fig. 11: Speed vs Wire Radius, of helix design graph for three different wavelengths and fixed inner radius. Dashed lines showcase the max t_d for h respective values. Equation 14 is used.

The final graph showcased in Figure 11 observes the relationship between the speed and the helix wire radius, across three values of h and with a fixed inner radius of 4 mm. To note in this figure are also the dashed lines which represent the moment that the wire radius becomes too large for a respective h, therefore turning the helix into a solid cylinder. As can be seen a larger wire radius is more beneficial to generating velocity, since after a certain size the amount of drag produced is overcome by the amount thrust. However, that point at the sizes being tested for the milli-robot capsule happens late. Therefore, an as small as possible wire radius is better. Despite it not generating thrust, it does not add to the drag of the body; therefore slowing it down.

Based on the following information it was decided the make the inner radius as large as possible at 11.25 mm, the wire radius as small as possible at 1 mm, and the h value as small as possible given the wire radius. The h value chosen was of 0.5 mm. As well, not showcased above, it was found out that the more turns the more beneficial it would be to the speed of the helix. Given the maximum length possible, it was opted that the helix would have 5 turns. This results in an overall length of the propeller approximately 15 mm. The final CAD design can be viewed in Figure 12.

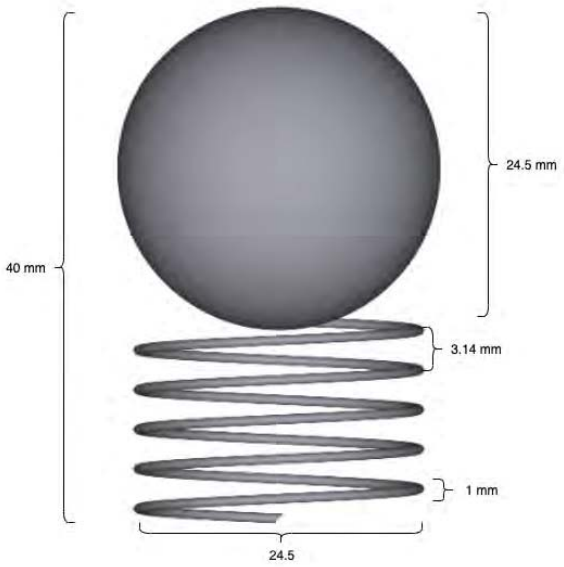

Fig. 12: Design of optimized helix milli-robot with inner diameter of 24.5 mm, wavelength of 3.14 mm, wire thickness of 1 mm, and total length of 40 mm.

3.7 Energy Conversion

As a result of the design choices made for both the helix and the screw milli-robots it is now possible to calculate the amount of work each design theoretically produces, as well as the efficiency it has in converting the magnetic energy provided by the test-setup.

Equations (18) and (19) are used to find the kinetic energy and work of the designs. All variables of interest are tabulated in Table 2 for simplicity of observation. Both milli-robot contain the same internal components, therefore containing the same weight in terms of micro-electronics. CAD models for both designs were given a 3D printable material to be able to obtain the respective mass of each design. Polycarbonate was chosen as the material due to its ability to be 3D printed, as well as being waterproof and rigid. Both are useful specifications as the material would be submerged in liquid and the body needed to stay rigid so that it would easily be able to swim. Using CAD models simulated with the material weight of the designs was estimated.

Work represents the change in kinetic energy from potential energy, as well as the amount of force multiplied by a displacement. Looking at the amount of work for each design, the results above can be interpreted as the following. Assuming both designs experience the same force, the helix design is able to

Table 2: Table of variables related to energy for each respective milli-robot design

Variables	Helix	Screw
Mass (g)	1.21	5.93
Velocity (mm/s)	0.8	0.45
Angular Velocity (rad/s)	$4.2{\cdot}10^{-3}$	$4.2{\cdot}10^{-3}$
Kinetic Energy (J)	$8.39{\cdot}10^{-9}$	$8.6{\cdot}10^{-9}$
Magnetic Energy (J)	$6{\cdot}10^{-6}$	$6{\cdot}10^{-6}$
Work (J)	$5.9951{\cdot}10^{-6}$	$5.9949{\cdot}10^{-6}$

travel a larger distance than the screw design. The above means that having the same magnetic energy, the helix design is better able to translate that energy into work; resulting in longer sustained motion.

4 DISCUSSION

4.1 Limitations of Models

The resistive force model does not respect trends at extremely low numbers, and both models do not take into consideration the weight of the body in its ability to generate speed. The aforementioned means that for the helix design a larger amount of variables which potentially could have yielded more performant results were not tested for. As well, given that the weight was not taken into account perhaps some of the designs, specifically the screw, would be too heavy to be turned by the torque provided from the set-up discussed in sections 4.1-2.

4.2 Further Work

Further work to be considered would be experimental testing to observe the extent that the mathematically derived designs above represent a real world situation. As well, another aspect of interest would be a comparison of rigid body and soft body designs to see which would be able better.

5 CONCLUSION

Resistive Force Theory and Oldroyd-B models were used to model the linear velocity of two milli-robot capsule designs. Both models at their core used an angular velocity derived from Stoke's drag, and a magnetic torque powered by tri-axial coils through powerful magnets. Design parameters were simulated in MATLAB to maximize the linear velocity of each milli-robot design. It was found that a screw design benefitted most from: a low wavelength distance, a low inner radius, a high arm depth, and a high number of starts. The helix design benefited most from a high inner radius, a low wavelength, and a low arm depth. Both designs benefited from having a higher number of turns. Once optimal parameters were found the designs ability to convert magnetic energy into work was evaluated. The helix design was found to able to produce more work given the same magnetic energy experienced by the screw. This was a result of the lower mass, as well as the higher linear velocity the design had. The conclusion to the research question is that a helix design is superior to a screw design when transforming magnetic potential energy into work.

REFERENCES

1. J.E.A. Wickham, Minimally invasive surgery: Future developments, *Bio Medical Journal*, (1994), 308(6922):193–195.
2. F. Gong, P. Swain, and T. Mills, Wireless endoscopy, *Gastrointestinal Endoscopy*, (2000), 51(6):725–729.
3. M. Chi, J. Zhang, R. Liu, Y. Wang, G. Nie, and X. Qian, Coupled steering control of a low torsional torque capsule robot in the intestine, *Mechatronics*, (2021), 77:102596.
4. B. Nelson, I.K. Kaliakatsos, and J.J. Abbott, Microrobots for minimally invasive medicine., *Annual review of biomedical engineering*, (2010), 12:55–85.
5. B. Huner and R. G. Hussey, Cylinder drag at low reynolds number, *The Physics of Fluids*, (1977), 20(8):1211–1218.
6. P.V. Bayly, B.L. Lewis, E. Ranz, R. Okamoto, R. Pless, and S. Dutcher, Propulsive forces on the flagellum during locomotion of chlamydomonas reinhardtii, *Biophysical journal*, (2011), 100:2716–25.
7. I.S.M. Khalil, A. Klingner, and S. MISRA, *Mathematical modeling of swimming soft microrobots*, ELSEVIER ACADEMIC Press, (2020). A. F. Tabak and S. Yesilyurt,
8. Improved kinematic models for two-link helical micro/ nanoswimmers, *Robotics, IEEE Transactions on*, (2014), 30:14–25.
9. N. Cohen and J. Boyle, Swimming at low reynolds number: A beginners guide to undulatory locomotion, *Contemporary Physics - CONTEMP PHYS*, (2010), 51:103–123.
10. L. Li and S.E. Spagnolie, Swimming and pumping by helical waves in viscous and viscoelastic fluids, *Physics of Fluids*, (2015), 27(2):021902.
11. Z. Zhang, A. Klingner, S. Misra, and I. S. M. Khalil, Control of magnetically-driven screws in a viscoelastic medium, In: *Proc.* , *2020 IEEE/RSJ International Conference on Intelligent Robots and Systems (IROS)*, (2020), 2840–2846.
12. E. Lauga, Propulsion in a viscoelastic fluid, *Physics of Fluids*, (2007), 19(8):083104.
13. American Society for Gastrointestinal Endoscopy, Capsule endoscopy, (2014).
14. F. Ullrich, F. Qiu, J. Pokki, T. Huang, S. Pané, and B. Nelson, Swimming characteristics of helical microrobots in fibrous environments, In: *Proc.* , (2016), 470–475.